Monthly Notices of the ROYAL ASTRONOMICAL SOCIETY

MNRAS **513,** 1834–1841 (2022) https://doi.org/10.1093/mnras/stac1014
Advance Access publication 2022 April 14

Long-term evolution of decayless kink oscillations of solar coronal loops

Sihui Zhong [1], Valery M. Nakariakov,[1]★ Dmitrii Y. Kolotkov[1] and Sergey A. Anfinogentov [2]

[1]*Centre for Fusion, Space and Astrophysics, Department of Physics, University of Warwick, Coventry CV4 7AL, UK*
[2]*Institute of Solar-Terrestrial Physics SB RAS, Irkutsk 664033, Russia*

Accepted 2022 April 7. Received 2022 March 29; in original form 2022 February 7

ABSTRACT

Long-term evolution of instantaneous parameters of decayless kink oscillations of six solar coronal loops observed for longer than 2 h each is studied. The oscillations are analysed by processing sequences of 171 Å images obtained with the Solar Dynamics Observatory (SDO)/Atmospheric Imaging Assembly (AIA) in the time interval from 2020 December till 2021 June, with the motion magnification technique. It is established that decayless kink oscillations could exist for more than 30 or 40 oscillation cycles. Neither the loop brightness nor instantaneous parameters of the oscillations show a monotonic increase or decrease during the oscillation. The observed instantaneous oscillation periods and amplitudes are found to vary randomly in time, with distributions around the mean values that resemble Gaussian profiles. Mean values of the oscillation periods and amplitudes are consistent with previous observations of this phenomenon. A power-law dependence of the oscillation period on the displacement amplitude is found, with the power-law index of 0.41 and with the 95 per cent confidence interval of [0.39, 0.71]. In general, we established the lack of correlation between instantaneous oscillation parameters and loop brightness. One exception is an event with relatively strong anticorrelation of the amplitude and the loop's brightness, with the cross-correlation coefficient of about −0.81, but this effect requires a further study. Fourier power spectra of the envelopes of the time-evolving instantaneous amplitudes and periods are white noise, indicating that consecutive values of the instantaneous parameters are independent of each other. The results obtained provide an empirical ground for validating and comparing existing and future theoretical models of decayless kink oscillations of coronal loops.

Key words: waves – Sun: corona – Sun: oscillations.

1 INTRODUCTION

It has been a decade since the first observation of the low-amplitude decayless kink oscillations of plasma structures of the solar corona, such as loops (Tian et al. 2012; Wang et al. 2012) and magnetic flux ropes (Kim, Nakariakov & Cho 2014). In coronal loops, the characteristic displacement amplitude of these persistent oscillations is 0.05–0.45 Mm and characteristic periods are 1.5–11 min (Anfinogentov, Nisticò & Nakariakov 2013; Anfinogentov, Nakariakov & Nisticò 2015). The linear scaling of the oscillation period with the length of the oscillating loop indicates that they are standing modes with the wavelength, and hence the oscillation period determined by the length of the oscillating loop acts as a kink wave resonator.

Appearing in the absence of eruptive events (Nisticò, Nakariakov & Verwichte 2013), and recognized to be ubiquitous in quiescent active regions (Anfinogentov et al. 2013, 2015), the decayless regime of kink oscillations has a great potential for coronal seismology (Duckenfield et al. 2018; Anfinogentov & Nakariakov 2019). In particular, it can provide us with the information about coronal active regions before the flares and mass ejections (e.g. Magyar & Nakariakov 2020; Nakariakov et al. 2021), which is crucial for the solar activity forecasting. Also, decayless kink oscillations may be useful in the broader context of the coronal heating problem (e.g. Van Doorsselaere et al. 2020), revealing unknown channels of the energy flow through the solar atmosphere. The potential of decayless kink oscillations for coronal heating through the development of Kelvin–Helmholtz instability (KHI) and resonant absorption is discussed by Karampelas et al. (2019a).

The mechanism responsible for sustaining the oscillations remains a mystery. In the large-amplitude decaying regime, in the vast majority of cases kink oscillations are impulsively excited by low coronal eruptions (Zimovets & Nakariakov 2015), with the follow-up damping caused by the conversion of the kink mode to unresolved torsional motions by resonant absorption (e.g. Goossens, Andries & Aschwanden 2002; Ruderman & Roberts 2002) or to fluting modes by KHI (e.g. Terradas, Magyar & Van Doorsselaere 2018; Antolin & Van Doorsselaere 2019; Van Doorsselaere et al. 2021). In contrast, due to its sustenance, decayless kink oscillations should be excited and sustained by a continuously operating external energy supply that counteracts damping. Nakariakov et al. (2016) demonstrated the lack of an apparent resonance in an ensemble of oscillating loops, which means that the force is not periodic. Two other options, a self-sustained oscillation with a quasi-steady energy supply and a decaying oscillation sustained by an external random driver, were proposed instead. To be more specific, in the randomly driven model, the footpoint driver varies rapidly and irregularly, in comparison with the kink oscillation period. Numerical simulations demonstrated that both options could lead to the existence of decayless kink oscillations (see Afanasyev, Karampelas & Van Doorsselaere 2019; Afanasyev, Doorsselaere & Nakariakov 2020; Karampelas & Van Doorsselaere 2020). The plausibility of the latter scenario has also been confirmed

★ E-mail: v.nakariakov@warwick.ac.uk

Table 1. Observation information of the analysed oscillating loops, including the NOAA active region (AR) number, the location of the image centre [(x, y) in arcsec from disc centre], the start time (t), time duration of the oscillation (Δt in hours), the length of the oscillating loop (L in Mm), and the mean period (P_0 in min) and amplitude (A_0 in Mm). The dash means the loop does not anchor at an active region.

Loop ID	AR	Date	(x, y) (arcsec)	t (UT)	Δt (h)	L (Mm)	P_0 (min)	A_0 (Mm)
Loop #1	12790	2020-12-12	(+838, −477)	10:30	3.2	210	4.32	0.23
Loop #2	–	2020-12-29	(−912, −366)	05:30	3.5	217	5.20	0.31
Loop #3	12796	2021-01-21	(+895, −371)	21:17	3.3	71	2.34	0.16
Loop #4	–	2021-03-23	(−778, −633)	05:24	4	181	4.72	0.23
Loop #5	–	2021-03-23	(−818, −620)	21:14	4.3	238	5.48	0.27
Loop #6	12833	2021-06-24	(+888, +393)	20:55	4.1	199	5.26	0.19

analytically by Ruderman & Petrukhin (2021) and Ruderman, Petrukhin & Pelinovsky (2021), while it could possibly depend on the noise spectrum. An alternative interpretation links decayless kink oscillations with regular, impulsively excited damped oscillations of loops with gradually evolving profiles of the equilibrium parameters (Antolin et al. 2016, 2017; Pascoe, Goddard & Van Doorsselaere 2020). These models involve the combination of resonant absorption and KHI.

A useful approach to revealing physical mechanisms operating in an oscillatory system is the comparison of empirically determined scaling of mean values of observables, such as the oscillation period, quality factor, amplitude, wavelength, etc., with each other with theoretically predicted mutual dependences of those parameters. In particular, such a comparison has revealed that the damping of kink oscillations is associated with the effect of resonant absorption (Ofman & Aschwanden 2002; Verwichte et al. 2013), their nature as eigen oscillations of individual coronal loops in both decaying and decayless regimes (Anfinogentov et al. 2015; Goddard et al. 2016), and the importance of non-linear effects (Goddard & Nakariakov 2016). For decayless kink oscillations, useful information could also come from the study of the evolution of their instantaneous parameters, for example the instantaneous values of the oscillation period and amplitude. The theoretical modelling of the mechanisms responsible for sustaining decayless kink oscillations has not predicted a scaling relationship between observables, but such a study could be motivated by the determination of the empirical scaling of the observed parameters of the oscillations.

The relatively low displacement amplitude of decayless kink oscillations, which is typically a fraction of a pixel size of the best available extreme ultraviolet (EUV) imaging telescopes, makes their study a rather challenging task. The technique of motion magnification (MM; Anfinogentov & Nakariakov 2016) has proven to be a robust tool for the analysis of this regime of coronal loop oscillations. It allows for a confident detection of transverse oscillatory motions with a broad range of oscillation periods in the plane of the sky, and gives a linear scaling of the output parameters of the oscillations with the input values (e.g. Zhong et al. 2021) even in noisy data. The MM has been successfully applied to the analysis of the second parallel harmonics (Duckenfield et al. 2018), and detection of preflare oscillations (Li et al. 2020; Mandal, Tian & Peter 2021).

The aim of this paper is to determine observational properties of decayless kink oscillations of coronal loops and their evolution during the lifetime of the oscillation. We expect that this empirical information would motivate the search for similar scaling laws in the theoretical modelling of the process, which would allow us to identify the specific mechanism responsible for the sustainability of the oscillations. The paper is organized as follows: in Section 2, we describe the observational data used in our study and the analytical technique; in Section 3, we present the results obtained; and in Section 4, we summarize our findings and draw conclusions.

2 OBSERVATIONS AND DATA ANALYSIS

For the analysis, we search for long-lasting (>2 h) decayless kink oscillations of high-contrasted coronal loops located off-limb or near limb in the time interval from 2020 January to 2021 June 25 using sequences of solar coronal images taken with the Atmospheric Imaging Assembly (AIA; Lemen et al. 2012). The analysed loops are situated in non-flaring, quiescent active regions, which prevents the appearance of decaying kink oscillations of the loops, driven by impulsive events. The observed coronal loops are most pronounced in the 171 Å channel and are less contrasted in cooler or hotter lines. Therefore, we only focus on the 171 Å data for the detection and analysis.[1] The analysed 171 Å AIA level 1 image sequences have the cadence time of 12 s and pixel size of 0.6 arcsec. The selected data (see Table 1) are processed with the Image Patch Extract routine to extract sub-frames with stationary patches. As the analysed features are off-limb, it is not necessary to derotate the image sequences.

2.1 Data analysis

As the amplitude of decayless kink oscillations is usually too small to be resolved by eye in movies made by AIA data sets (e.g. Anfinogentov et al. 2015; Nakariakov et al. 2021), we apply the MM technique to the AIA image sequences to magnify these subtle motions. In our study, parameters of the MM algorithm are determined according to a specific occasion, with the magnification factor k varying from 2 to 10, and smoothing width equals to 50 frames as the typical period of decayless kink oscillations is shorter than 10 min (Anfinogentov et al. 2015; Anfinogentov & Nakariakov 2019). The data with magnified oscillatory motions is used for the following analysis.

Each loop of interest is outlined by several clicked points, which are fitted to an ellipse. To cover the range of user-supplied points, the ellipse is truncated as an arc, whose length (chordal distance) is estimated as the loop length by summing up finite linear segments. Then, slits with a certain length and width are chosen perpendicular to the best-fitting ellipse to make time–distance plots in a similar manner as described in Duckenfield et al. (2018) and Anfinogentov & Nakariakov (2019). For each analysed loop, we have several slits across it, spaced evenly along the loop. The length of each specific slit is determined to include the full oscillatory transverse displacement of the loop of interest. At each instant of time, the transverse intensity

[1]Multithermal characteristics of kink oscillating loops are investigated by Nisticò, Anfinogentov & Nakariakov (2014).

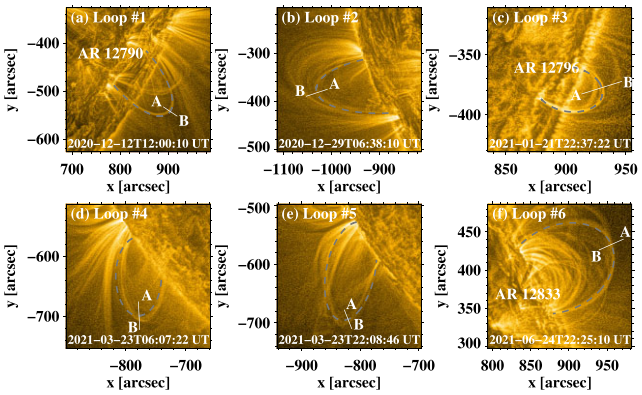

Figure 1. Overview of the selected coronal loops in which decayless kink oscillations are studied. Grey dashed curves are the best-fitting ellipses that highlight the loops. The white slits 'A–B' perpendicular to the ellipse are used to make time–distance plots that are presented in Fig. 2. Here, images are enhanced using the multiscale Gaussian normalization (Morgan & Druckmüller 2014).

profile is averaged over the slit width (usually several pixels) to enhance the signal-to-noise ratio. Such an averaging should not lead to any loss of information, as the oscillation wavelengths are comparable to the length of the oscillation loop, i.e. much larger than several pixels. In this way, time–distance data cubes (time, distance, slit number) are created. Next, we check the resulting time–distance cubes to see whether there is a clear decayless oscillatory pattern. If there is one, then the candidate is counted as a good example for further analysis.

For those candidate events with apparent decayless kink oscillations, we select one time–distance map with a clear oscillatory pattern as representative to analyse the evolution of decayless kink oscillations in this loop. Then oscillation parameters are measured with the use of the chosen time–distance plots as follows. First, in the time–distance plot, we track the loop boundary manually (by eye). Alternatively, we track the vibration of the loop centre by fitting the transverse intensity profile with a Gaussian at each instant of time, using the Solar Bayesian Analysis Toolkit (SOBAT; Anfinogentov et al. 2021).

Secondly, in the time–distance plot, we identify the maximum/minimum displacement positions (crests and troughs) of the transverse oscillation, $[t_i, d_i]$, where i is the extremum index, and t and d are the time and spatial coordinates, respectively. Thirdly, we calculate the instantaneous half-period ($P_i/2 = t_{i+1} - t_i$) and the magnified apparent instantaneous displacement amplitude (i.e. the distance between the crests and troughs, $2A_{\rm mi} = |d_{i+1} - d_i|$) for each half-cycle of oscillation. Since the magnified amplitude depends linearly on the original amplitude (Anfinogentov & Nakariakov 2016; Zhong et al. 2021), the original apparent amplitude is $1/k$ of the magnified amplitude, i.e. $A_i = A_{\rm mi}/k$. To reduce the uncertainty, we repeat the above procedure for magnified data obtained with three different magnification factors k, e.g. $k = 4$, 6, 8. In this way, we obtain a sequence of pairs of the instantaneous half-periods $P_i/2$ and amplitudes $2A_i$ determined for consecutive half-cycles with different values of k, which are used in statistical analyses.

3 RESULTS

We analyse decayless kink oscillations of six loops selected according to the high contrast and long-durational oscillatory patterns.

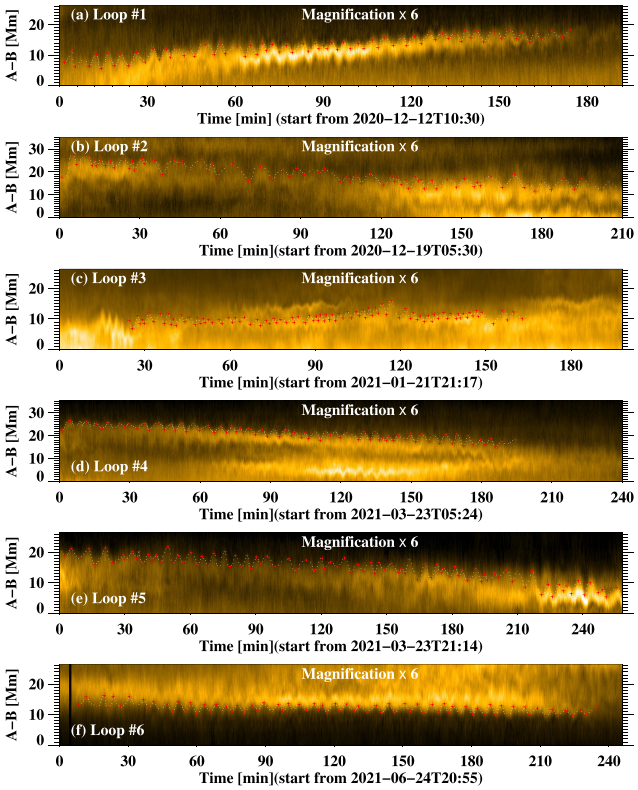

Figure 2. Typical time–distance maps demonstrating decayless kink oscillations in the analysed loops. The maps are made using the slits situated across the loops, denoted in Fig. 1. In all cases, the magnification factor k of the magnified data is 6. The white dots represent the apparent loop boundary in the plane of the sky, and the red crosses denote the maximum/minimum displacement of the loop boundary. In panel (f), the dark vertical slit corresponds to dark frames, i.e. the missing data frames. In each panel, the intensity is scaled to reveal the oscillatory pattern. Animation shows the oscillations of Loop #1 and a time–distance map with (left) and without (right) the MM.

The overviews of the host active regions are displayed in Fig. 1. The information about the loops and the dates and times of the observations is shown in Table 1. It includes the NOAA active region (AR) number, coordinates of the region of interest, the observation date and start time and duration, the oscillating loop length, the mean value of oscillation period, and amplitude. Among these six loops, three of them are anchored in active regions that have NOAA numbers. Loop #4 and Loop #5 are from the same decaying active region. Most of their (apparent) footpoints are near the limb, some are located on disc, while others are beyond the limb. All loops are seen in 171 Å for longer than 3 h. Their lengths vary from 71 Mm (62 Mm) to 238 Mm. Loop #3 gets split into two threads at about 1/3 of observation, with one of the 71 Mm length moving upwards, see the oscillatory pattern above the fitted one in the time–distance map in Fig. 2(c); while another one of 62 Mm oscillating around the initial position. But, though both of these new loops are anchored at the same footpoints, they may simply overlap due to the line-of-sight (LoS) effect, and as the Sun rotates westwards, one grows longer visually.

Fig. 2 shows examples of time–distance plots made along identified perpendicular slits labelled by 'A–B' in Fig. 1. In each example, the oscillating loop remains high contrasted even if its intensity varies in time, so the transverse profile of the loop is recognizable most of the time, hence the oscillatory pattern. In the vicinity of

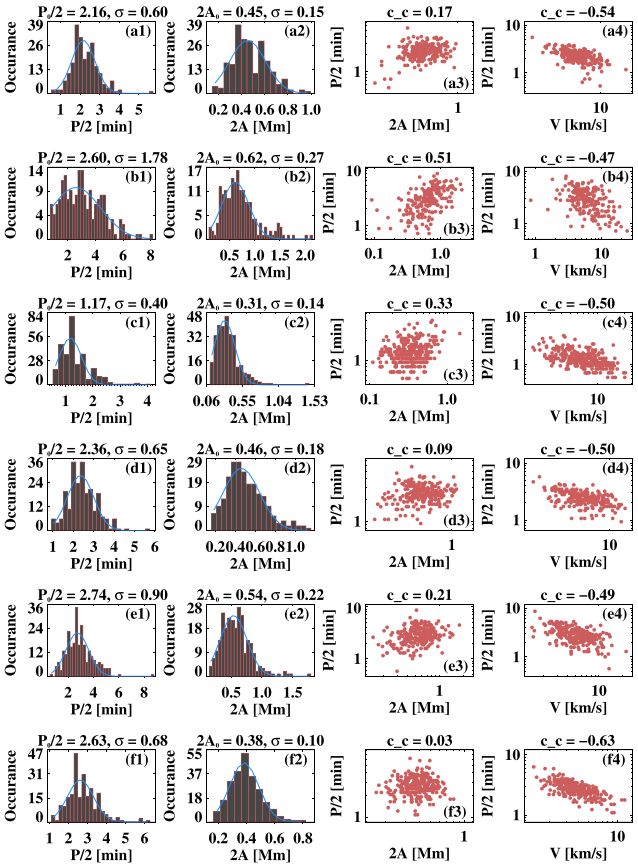

Figure 3. Instantaneous oscillation amplitudes ($2A$) and periods ($P/2$) of decayless kink oscillations in six coronal loops, with rows from top to bottom corresponding to Loop #1 to Loop #6. The histograms of half-periods (first column) have 0.2 min bins, and of amplitude (second column) have 0.05 Mm bins. Scatter plots of the amplitude–period pairs and velocity amplitude (V)–period pairs on logarithmic scales are given in the third and fourth columns, respectively. The blue curves represent the best-fitting Gaussians to the histograms, with the centres and widths of the Gaussian fits indicated in the corresponding panels. The cross-correlation coefficients (c_c) between parameter pairs are indicated at the top of each scatter plot.

Loop #4, there is another distinguishable loop that has a pronounced oscillation signal that lasts for around 2 h, see the oscillatory pattern in the bottom of the panel (d). The white dots outline one of the boundaries of the loop, and the red crosses indicate positions of the extreme displacements. In all cases, transverse oscillations last for tens of cycles. More specifically, the oscillations of Loop #1 to Loop #6 sustain for 38, 38, 48, 40, 47, and 26 cycles, respectively. In all the cases, the instantaneous oscillation period, i.e. the duration of one cycle is about several minutes. The visual inspection reveals that the instantaneous amplitude and period vary in time. Focusing on one certain case, these oscillation parameters evolve slowly, with minor increase or decrease in time. However, oscillations of Loop #1 and Loop #6, have a virtually stationary period and their amplitude do not vary too much, as seen in panels (a) and (f).

3.1 Instantaneous parameters of the oscillations

Histograms of instantaneous displacement amplitudes and periods determined during the time evolution of the six analysed loops, are shown in Fig. 3. The histograms generally have a Gaussian (normal) distribution. Best-fitting the distribution with the Gaussian

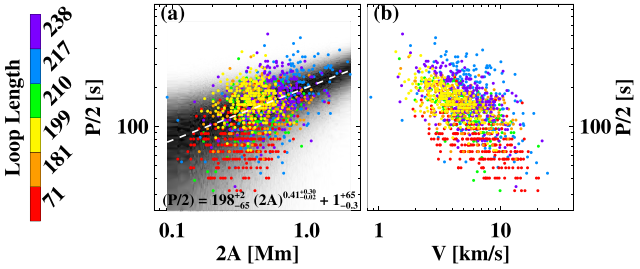

Figure 4. Scatter plots of instantaneous displacement amplitudes and periods (panel a) and instantaneous velocity amplitudes and periods (panel b) of decayless kink oscillations observed in six different loops. Circles of green, blue, red, orange, purple, and yellow correspond to Loop #1 to Loop #6, respectively. The colour bar in the left indicates the loop length (in Mm) of different oscillating loops. The white dashed line shows the best-fitting line, corresponding to the power-law dependence shown at the bottoms of panel (a). The background is the posterior predictive distribution sampled by MCMC for the best-fitting power function.

function, we determine centres and standard deviations of the Gaussian fits. The centres give us the mean values of the oscillation parameters. For Loop #1 to #6, their oscillation periods ($P_0 \pm \sigma$) are 4.32 ± 1.2, 5.20 ± 3.54, 2.34 ± 0.80, 4.72 ± 1.3, 5.48 ± 1.8, and 5.26 ± 1.36 min, respectively, and their apparent amplitude ($A_0 \pm \sigma$) is 0.23 ± 0.075, 0.31 ± 0.135, 0.16 ± 0.07, 0.23 ± 0.09, 0.27 ± 0.11, and 0.19 ± 0.05 Mm, respectively. The errors are estimated by the standard deviations. Loop #2 has the widest spread of the period and amplitude, while the smallest deviations of those parameters are in Loop #3 and Loop #6, respectively.

The correlation between the instantaneous oscillation periods and apparent amplitudes is studied with the use of scatter plots of those two variables with each other on a logarithmic scale (see the third column in Fig. 3). In addition, we calculate cross-correlation coefficients of the period and amplitude time evolutions. It is found that the cross-correlation coefficients in Loop #1 and Loop #3–Loop #6 are less than 0.35, i.e. negligibly small, while in Loop #2 it is 0.51 that may indicate some meaningful correlation. Since the velocity amplitude (V, estimated as $2\pi A/P$) is a proxy of oscillation energy, similar scatter plots of periods and velocity amplitude are created [see panels (a4)–(f4)] to reveal the power-law dependence of the velocity amplitude (and the kinetic energy) upon the period. Cross-correlation coefficient between these two variables in Loop #1 to Loop #6 is −0.54, −0.47, −0.46, −0.50, −0.49, and −0.63, respectively, indicating weakly negative correlation. In addition, two scatter plots that combine the measurements made in all six loops are shown in Fig. 4. Parameters of different loops are indicated by a certain colour. As kink oscillations are of standing nature, their period should linearly scale with the loop length, which can be roughly seen in Fig. 4. As a matter of fact, the estimation of the loop length is subject to the projection effect, and more accurate estimations could be done with stereoscopic data not available in the considered cases. The cross-correlation coefficient of oscillation periods and amplitudes estimated in all six loops is 0.42, and that of periods and velocity amplitudes is −0.46.

As the cross-correlation coefficients of data-pairs do not show a conclusive relationship between oscillation parameters of interest, while scatter plots in Fig. 3 show that power-law dependence between amplitude and period is highly possible, we perform a quantitative comparison of two competing models with the use of SOBAT. The models are (1) the power-law model, $P = c(A)^{\alpha} + P_0$, where P and A are the period and displacement amplitude, respectively, c

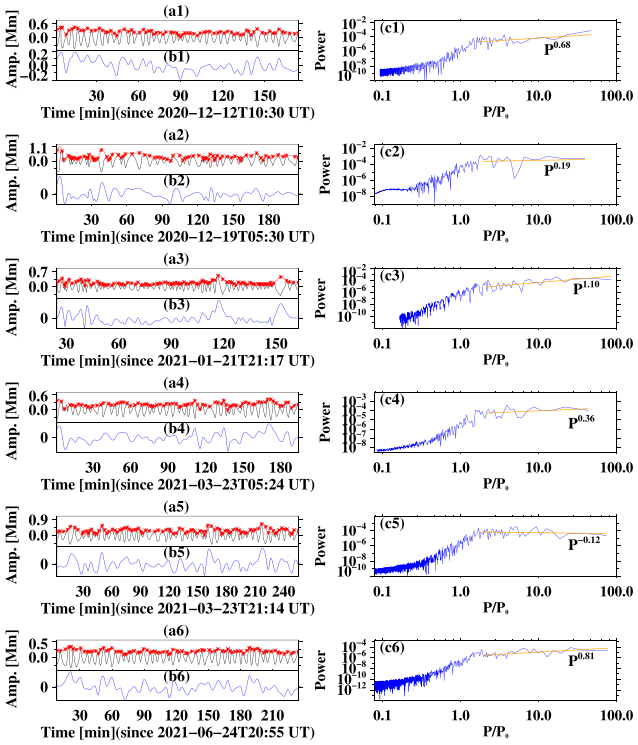

Figure 5. Time evolution of the instantaneous amplitudes of decayless kink oscillations. Panels (a1)–(a6): detrended time series of the instantaneous amplitudes (black curve) obtained by subtracting the trend from oscillating signal indicated by white dots in Fig. 2, and their envelops (red curves) obtained by interpolating the absolute values of the detrended crests and troughs (red stars) with cubic splines. Panels (b1)–(b6): centred envelops extracted from panels (a1)–(a6). Panels (c1)–(c6): Fourier power spectra of the time evolution of the envelopes. The orange lines are best-fitting linear functions of the spectra. The corresponding fitting coefficients are labelled. The periods are normalized to the mean values obtained in Fig. 3.

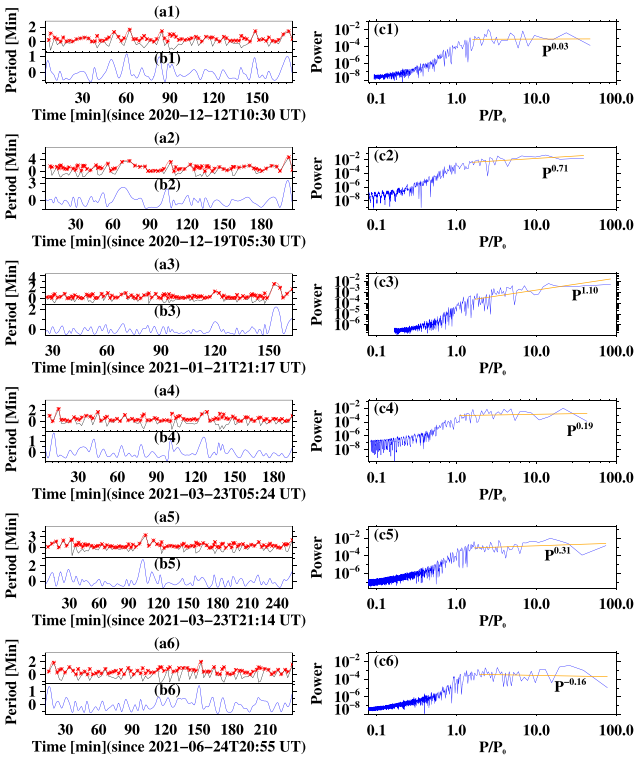

Figure 6. Similar to Fig. 5 but for instantaneous periods.

is a normalization constant, α is a power-law index, and P_0 is an intercept constant term and (2) the flat model, $P = P_0$, i.e. the period is independent of displacement amplitude. For all six loops together, data-pairs are best fitted with these two competing models separately using the Markov chain Monte Carlo (MCMC) approach with 10^6 samples, and the Bayesian evidence is calculated. Then, the Bayes factor B_{12} is estimated as the ratio of the Bayesian evidence of the two models. Thus, we obtain the value $K_{12} = 2\ln B_{12}$, as a measure of how strong the evidence towards model 1 with respect to model 2 is. For all six loops together, K_{12} of 9.65 yields strong evidence in favour of the power-law model in comparison to the flat model. The best-fitting power-law index $\alpha = 0.41$, with the 95 per cent confidence interval of [0.39, 0.71]. The best-fitting curve is shown in Fig. 4, overplotted with corresponding posterior predictive distribution sampled by MCMC, which is well consistent with observations. Here, as velocity amplitude is proportional to A/P, the dependence between it and the period can be inferred from that of the period and displacement amplitude. Hence, there is no need to perform additional fitting of these two parameters.

3.2 Time evolution of the instantaneous parameters

In Section 3.1, we found that the instantaneous oscillation periods and amplitude have a Gaussian-like distributions. However, the histograms do not give us the information about whether this variation of the oscillation parameters is abrupt or gradual. To reveal the time evolution of the oscillation parameters, we determine the gradual trend of the oscillations by smoothing the mid-points of the extreme positions of the oscillatory displacements, indicated by the red crosses in Fig. 2, with a window width of around double the period. Then the trend was subtracted from the signals to obtain the detrended time series, see the black curves in Fig. 5(a1)–(a6). Interpolated time envelopes of the oscillation parameters are shown by blue curves. It is evident that the amplitude and period vary in time rather smoothly, while irregularly. The time evolution of the instantaneous parameters is quantified by the Fourier power spectra. For the analysis, it is convenient to construct an envelope that spline interpolates the absolute values of detrended extremes (i.e. both maxima and minima, see the red stars in Fig. 5a). Power spectra of the envelopes of instantaneous amplitudes and periods are shown in Figs 5 and 6, respectively, with the periods measured in the values of the corresponding mean oscillation periods P_0 obtained in Fig. 3.

The power spectra are broadband. Typically, the spectra have three distinct intervals that could be fitted with linear functions that correspond to the power-law dependences of the spectral power. Obviously, the meaningful spectral intervals for this fitting are with the periods greater than P_0. For the instantaneous amplitudes, the best-fitting values of the power-law indices are 0.68, 0.19, 1.10, 0.36, −0.12, and 0.81 for Loop #1 to #6, respectively. The average value is 0.50 and the standard deviation is 0.44, giving the spectrum resembling white noise. A similar behaviour is shown by the evolution of the instantaneous periods (Fig. 6). In the long-period part of the spectra, the best-fitting power-law indices are 0.03, 0.71, 1.10, 0.19, 0.31, and −0.16, giving us the mean value of 0.36 and the standard deviation of 0.46. Thus, the spectrum of the time variation of the instantaneous periods is close to the white noise too.

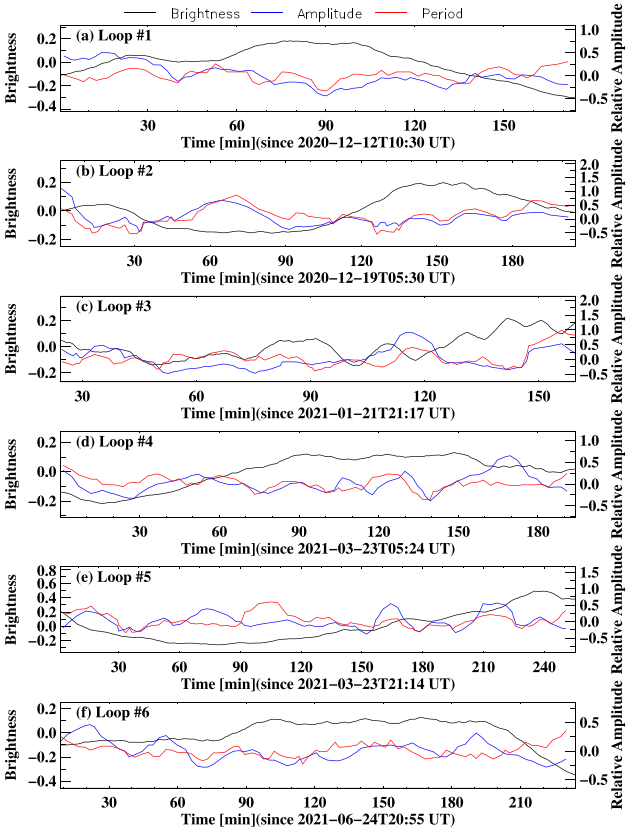

Figure 7. Time variation of the relative instantaneous brightnesses (black curves), and oscillation amplitudes (blue curves) and periods (red curves) of six oscillating loops. All curves are smoothed over five oscillation half-cycles.

3.3 Correlation of the oscillation parameters with the brightness of the loop

According to Fig. 2, the instantaneous brightness of the oscillating loops varies in time. It is of interest to test whether the variation of instantaneous parameters of the oscillations correlates with the loop's brightness. For example, Loop #1 becomes brighter in the middle of the observation, while the oscillation amplitude turns apparently smaller. In each time frame, the brightness is estimated as the maximum value in the perpendicular slit shown in Fig. 1. Here, the instantaneous brightness of a loop's centre is the original one with mean value subtracted and then normalized by the average brightness of the loop during the whole duration of the observation. The time variations of the brightness and simultaneous variations of instantaneous periods and amplitudes in all analysed loops are shown in Fig. 7. The brightness trends in different loops are different, while intermittent minor changes are seen in all six loops. Loop #1 brightens up gradually and then dims quicker. Loop #2 turns dimmer in the middle. Brightness of Loop #3 varies frequently. Loop #4 and Loop #5 grow brighter at the end of observation. The brightness of Loop #6 sustains for more than 2 h but drops down rapidly in the end of the observation.

Generally, the evolution of oscillation parameters and loop brightness are not synchronized. In all six loops, cross-correlation coefficients between the brightness and amplitude or period for the full series do not exceed 0.5. However, in three events, in some specific time intervals there exists negative correlation between brightness and displacement amplitude. The cross-correlation coefficient between the brightness and amplitude for Loop #1 in the time interval of [0, 123 min] is −0.81, for Loop #2 in [53 min, 136 min] is −0.74, and for Loop #5 in [71 min, 156 min] is −0.72.

4 DISCUSSION AND CONCLUSIONS

In our study, we considered instantaneous parameters of decayless kink oscillations in six long-living (>2 h) coronal loops. All the analysed loops appear in the 171 Å channel of SDO/AIA are off-limb, and have contrast boundaries with the background. During the chosen time intervals, the loops show decayless low-amplitude oscillatory transverse displacements. The observed oscillatory patterns last in the six different loops for 38, 38, 48, 40, 47, and 26 oscillation cycles. The oscillations can occur for much longer, and are not detected outside the analysed time intervals because of the change of the observational conditions. Observational data cubes were processed with the use of the MM technique (Anfinogentov & Nakariakov 2016), which allows us to magnify oscillatory motions in a broad range of periods and amplitudes (Zhong et al. 2021). We determine instantaneous values of the oscillation amplitudes and periods as the distances and times between extreme values of repetitive transverse displacements of the loops. The amplitudes are apparent, i.e. the effect of the angle between the LoS and the unknown plane of the oscillation, if the oscillations are linearly or highly elliptically polarized, is not taken into account. In all the analysed loops, the oscillation amplitudes do not show a systematic decay or growth.

Mean values of the oscillation periods determined in different loops are 4.32 ± 1.2, 5.20 ± 3.54, 2.34 ± 0.8, 4.72 ± 1.3 , 5.48 ± 1.8, and 5.26 ± 1.36 min, and the corresponding apparent amplitudes are 0.23 ± 0.075, 0.31 ± 0.135, 0.16 ± 0.07, 0.23 ± 0.09, 0.27 ± 0.11, and 0.19 ± 0.05 Mm. The error bars were estimated by the standard deviation. Parameters of the analysed oscillations are fully consistent with previous observations of this phenomenon by, e.g. Nisticò et al. (2013), Anfinogentov et al. (2013, 2015), Anfinogentov & Nakariakov (2019), and Li et al. (2020).

Instantaneous values of both the oscillation amplitudes and periods show scattering around the mean values. In all six loops, histograms of the instantaneous oscillation parameters have Gaussian-like distributions, while in some cases there are significant outlets. Some strong outlets in the instantaneous periods could be attributed to oscillation cycles that are missing in the detection, when, because of noise it is impossible to identify extreme values of the displacements. Strong outlets in instantaneous amplitudes could be attributed to the effect of evolving background intensity.

The variance of oscillation parameters varies from loop to loop. There may be some correlation with the host active region, e.g. their magnetic complexity. For example, Loop #1 and Loop #6 have periods and amplitudes that fluctuate not too much, and both are in a unipolar active region that share similar properties (e.g. the size of the active region, spot numbers). However, Loop #2, Loop #4, and Loop #5 are located in decaying active regions that contain no sunspots; hence, no proxy to quantify the properties of their host regions. Similarly, Loop #3 is anchored at an active region where a sunspot is disappearing during the observation, which indicates a low potential for flares. Therefore, the link between the variation of oscillation parameters and properties of the host active region is not obvious in the current work, and it would be more suitable to be investigated in statistics containing tens of cases in the future.

In previous observation of decayless kink oscillations of coronal loops, the oscillation period was found to be independent of amplitude (e.g. Nakariakov et al. 2016). In all loops analysed in our study except one, cross-correlation coefficients of the instantaneous periods and amplitudes are lower than 0.5. In one loop, its value

is 0.51. The visual inspection of a scatter plot that combines the instantaneous parameters of all oscillatory cycles in all six loops may suggest some positive correlation of these parameters with each other. However, the small value of the cross-correlation coefficient, 0.42, does not allow us to claim this correlation confidently. Likewise, the negative correlation between velocity amplitude and period cannot be confirmed by their cross-correlation coefficients of −0.46 to −0.63. On the other hand, using the MCMC Bayesian approach, we found strong evidence that the oscillation period has indeed a power-law dependence on displacement amplitude, with power-law index of $0.41^{+0.30}_{-0.02}$, through quantitative comparison of best-fitting models for P versus A for all six loops among flat model and power-law model.

The scattering of instantaneous parameters of the oscillations should rather be attributed to the usual random scattering of experimental data because of noise, intrinsic to any natural phenomenon. On the other hand, the marginal indication of the positive correlation of the instantaneous amplitudes and periods does not fully exclude a possibility of a true dependence that should be looked for in bigger data sets. Such a correlation should also be searched for in the competing theoretical models of decayless kink oscillations. Likewise, the Gaussian distributions of the instantaneous periods and amplitudes could be looked for in the model suggested by Afanasyev et al. (2020); i.e. it should be checked whether such statistics are purely based on the observational errors, or are features of the model. The width of the Gaussian distribution determined in our study empirically could be compared with the width determined by the model parameters, e.g. the statistics of the random driver.

Looking at the time evolution of the instantaneous parameters of the oscillations, i.e. the time envelopes, we established that in all cases its Fourier power spectra in the intervals of the oscillation periods greater than the mean period are power law with the indices of 0.68, 0.19, 1.10, 0.36, −0.12, and 0.81 for instantaneous amplitudes and 0.03, 0.71, 1.10, 0.19, 0.31, and −0.16 for instantaneous periods. The mean value of the power-law index of the envelope of the instantaneous amplitudes is 0.50 ± 0.44, and of the period is 0.36 ± 0.46. We interpret those spectra as almost white noise. Thus, we do not see a significant correlation of the instantaneous values of the amplitudes in consecutive cycles of the oscillations. The same is applicable to instantaneous periods. Therefore, we conclude that decayless kink oscillations do not form oscillation trains, in contrast with another almost monochromatic oscillatory process in the solar atmosphere, 3-min oscillations above sunspot umbrae (e.g. Sych 2016). This feature of decayless kink oscillations could also be important for the identification of the specific mechanisms responsible for their sustainability. What should also be taken into account is that the loop, in reality, is subject to a combination of regular and noisy external perturbations, which affects the statistics.

The brightness of the observed loops in the 171 Å channel shows some time variation. In general, we did not find a correlation of the brightness variation with the variation of the instantaneous periods and amplitudes of the oscillations. However, statistically significant anticorrelation of the brightness and amplitude, with the highest cross-correlation coefficient of about −0.81, was established in some specific time interval for one of the loops. The apparent independence of the instantaneous period of the brightness suggests that the variation of the brightness does not modify the kink speed in the loop. It means that either the brightness variation does not involve the variation of the magnetic field and density, or they both evolve but their evolution does not change the ratio of the field and the square root of the density. The appearance of significant anticorrelation of the brightness and oscillation amplitude in a certain time interval may be attributed to the selection effect and thus be artificial. However, we cannot rule out its natural origin, which indicates a need for a dedicated study of this effect.

The apparent sustainability of the oscillations for much longer than 30–40 oscillation cycles, with the intensity varying non-monotonically, indicates that the KHI mechanism may not play the main role in this process. The instability caused by the transverse shear of flows in the oscillations has been intensively studied in numerical simulations (e.g. Antolin et al. 2016; Afanasyev et al. 2019; Guo et al. 2019; Karampelas et al. 2019a; Karampelas, Van Doorsselaere & Guo 2019b). In these simulations, once being excited by a continuous footpoint driver, the loop starts oscillating and the oscillation amplitude first grows until the onset of turbulence/KHI, and then decays due to energy dissipation via KHI (see e.g. figs 7 and 8 in Guo et al. 2019). For example, the time-scale of this growth–decay process is 1500–2000 s (14–17 cycles of the oscillation), given the driver velocity of 2 km s^{-1}, period of 87–106 s, and magnetic field of 50 G. However, in our observations, the oscillation amplitude sustains for much longer than 20 cycles along with reversible evolution of the loop width and intensity. In addition, the intensity variation in the host loops caused by KHI should be positively related to the apparent amplitude changes in 171 Å and be negatively related in a hotter line like 193 Å (Antolin et al. 2016), but Fig. 7 show that there is no correlation between the loop brightness and the oscillation amplitude or period. Yet, whether KHI is visible in EUV image sequence depends on the initial boundary condition of coronal loops (Antolin et al. 2017). If the temperature inside and outside the loop is similar, the overall intensity variation as response of KHI is minor, which could be in an undetectable spatial scale. Anyway, our findings offer important observational evidence for the further study of the possible appearance of KHI in decayless kink oscillations of coronal loops.

Empirical results obtained in this study show that decayless kink oscillations of coronal loops could exist for more than 30 or 40 oscillation cycles. Neither the loop brightness nor instantaneous parameters of the oscillations show a systematic evolution during the analysed time intervals. We established the lack of correlation between instantaneous oscillation period and amplitude, and, in general, between the oscillation parameters and loop brightness. One exception could be a relatively strong anticorrelation of the oscillation amplitude and the loop's brightness, but this effect requires a further study. Furthermore, period and displacement amplitude could have a power-law dependence, of which physical implication remains uncertain. Anyway, due to the size of the associated uncertainties, it is difficult to unequivocally stipulate the precise relationship. Consecutive values of the instantaneous parameters of the oscillations are independent of each other. The variation of the instantaneous parameters seems to be purely random, and hence needs to be considered as an observational error. These results indicate the questions that should be addressed by the existing and future theoretical models of the phenomenon of decayless kink oscillations of coronal loops.

ACKNOWLEDGEMENTS

SZ gratefully acknowledges fruitful discussions with Dr Timothy Duckenfield on MCMC fitting, and support from China Scholarship Council–University of Warwick joint scholarship. Data are courtesy of the SDO/AIA team.

DATA AVAILABILITY

In this paper, we analysed AIA data using the Interactive Data Language (IDL), SolarSoftWare (SSW; Freeland & Handy 1998) package, the MM technique (Anfinogentov & Nakariakov 2016), and the Solar Bayesian Analysis Toolkit (SOBAT; Anfinogentov et al. 2021). The AIA data are available at http://jsoc.stanford.edu/. The data are processed and analysed using the routines available at https://www.lmsal.com/sdodocs/doc/dcur/SDOD0060.zip/zip/entry/ (Section 7). The MM code is available at https://github.com/Sergey-Anfinogentov/motion_magnification. The SOBAT is available at https://github.com/Sergey-Anfinogentov/SoBAT/tree/master/idl.

REFERENCES

Afanasyev A. N., Karampelas K., Van Doorsselaere T., 2019, ApJ, 876, 100
Afanasyev A. N., Doorsselaere T. V., Nakariakov V. M., 2020, A&A, 633, L8
Anfinogentov S. A., Nakariakov V. M., 2016, Sol. Phys., 291, 3251
Anfinogentov S. A., Nakariakov V. M., 2019, ApJ, 884, L40
Anfinogentov S. A., Nisticò G., Nakariakov V. M., 2013, A&A, 560, A107
Anfinogentov S. A., Nakariakov V. M., Nisticò G., 2015, A&A, 583, A136
Anfinogentov S. A., Nakariakov V. M., Pascoe D. J., Goddard C. R., 2021, ApJS, 252, 11
Antolin P., Van Doorsselaere T., 2019, Front. Phys., 7, 85
Antolin P., De Moortel I., Van Doorsselaere T., Yokoyama T., 2016, ApJ, 830, L22
Antolin P., De Moortel I., Van Doorsselaere T., Yokoyama T., 2017, ApJ, 836, 219
Duckenfield T., Anfinogentov S. A., Pascoe D. J., Nakariakov V. M., 2018, ApJ, 854, L5
Freeland S. L., Handy B. N., 1998, Sol. Phys., 182, 497
Goddard C. R., Nakariakov V. M., 2016, A&A, 590, L5
Goddard C. R., Nisticò G., Nakariakov V. M., Zimovets I. V., 2016, A&A, 585, A137
Goossens M., Andries J., Aschwanden M. J., 2002, A&A, 394, L39
Guo M., Van Doorsselaere T., Karampelas K., Li B., Antolin P., De Moortel I., 2019, ApJ, 870, 55
Karampelas K., Van Doorsselaere T., 2020, ApJ, 897, L35
Karampelas K., Van Doorsselaere T., Pascoe D. J., Guo M., Antolin P., 2019a, Front. Astron. Space Sci., 6, 38
Karampelas K., Van Doorsselaere T., Guo M., 2019b, A&A, 623, A53
Kim S., Nakariakov V. M., Cho K. S., 2014, ApJ, 797, L22
Lemen J. R. et al., 2012, Sol. Phys., 275, 17
Li D., Li Y., Lu L., Zhang Q., Ning Z., Anfinogentov S., 2020, ApJ, 893, L17
Magyar N., Nakariakov V. M., 2020, ApJ, 894, L23
Mandal S., Tian H., Peter H., 2021, A&A, 652, L3
Morgan H., Druckmüller M., 2014, Sol. Phys., 289, 2945
Nakariakov V. M., Anfinogentov S. A., Nisticò G., Lee D. H., 2016, A&A, 591, L5
Nakariakov V. M. et al., 2021, Space Sci. Rev., 217, 73
Nisticò G., Nakariakov V. M., Verwichte E., 2013, A&A, 552, A57
Nisticò G., Anfinogentov S., Nakariakov V. M., 2014, A&A, 570, A84
Ofman L., Aschwanden M. J., 2002, ApJ, 576, L153
Pascoe D. J., Goddard C. R., Van Doorsselaere T., 2020, Front. Astron. Space Sci., 7, 61
Ruderman M. S., Petrukhin N. S., 2021, MNRAS, 501, 3017
Ruderman M. S., Roberts B., 2002, ApJ, 577, 475
Ruderman M. S., Petrukhin N. S., Pelinovsky E., 2021, Sol. Phys., 296, 124
Sych R., 2016, Washington DC American Geophysical Union Geophysical Monograph Series, 216, 467
Terradas J., Magyar N., Van Doorsselaere T., 2018, ApJ, 853, 35
Tian H., McIntosh S. W., Wang T., Ofman L., Pontieu B. D., Innes D. E., Peter H., 2012, ApJ, 759, 144
Van Doorsselaere T. et al., 2020, Space Sci. Rev., 216, 140
Van Doorsselaere T., Goossens M., Magyar N., Ruderman M. S., Ismayilli R., 2021, ApJ, 910, 58
Verwichte E., Van Doorsselaere T., White R. S., Antolin P., 2013, A&A, 552, A138
Wang T., Ofman L., Davila J. M., Su Y., 2012, ApJ, 751, L27
Zhong S., Duckenfield T. J., Nakariakov V. M., Anfinogentov S. A., 2021, Sol. Phys., 296, 135
Zimovets I. V., Nakariakov V. M., 2015, A&A, 577, A4

This paper has been typeset from a TEX/LATEX file prepared by the author.